ADVANCED FUNCTIONAL MATERIALS
www.afm-journal.de

Particle-Free Emulsions for 3D Printing Elastomers

Brittany M. Rauzan, Arif Z. Nelson, Sean E. Lehman, Randy H. Ewoldt, and Ralph G. Nuzzo**

3D printing is a rapidly growing field that requires the development of yield-stress fluids that can be used in postprinting transformation processes. There is a limited number of yield-stress fluids currently available with the desired rheological properties for building structures with small filaments (≤l00 µm) with high shape-retention. A printing-centric approach for 3D printing particle-free silicone oil-in-water emulsions with a polymer additive, poly(ethylene oxide) is presented. This particular material structure and formulation is used to build 3D structure and to pattern at filament diameters below that of any other known material in this class. Increasing the molecular weight of poly(ethylene oxide) drastically increases the extensibility of the material without significantly affecting shear flow properties (shear yield stress and linear viscoelastic moduli). Higher extensibility of the emulsion correlates to the ability of filaments to span relatively large gaps (greater than 6 mm) when extruded at large tip diameters (330 µm) and the ability to extrude filaments at high print rates (20 mm s^{-1}). 3D printed structures with these extensible particle-free emulsions undergo postprinting transformation, which converts them into elastomers. These elastomers can buckle and recover from extreme compressive strain with no permanent deformation, a characteristic not native to the emulsion.

1. Introduction

3D printing is a rapidly expanding field due to the ability to fabricate customizable structures with applications for actuators,[1] soft robotics,[2] tissue engineering,[3] and electronics.[4] The majority of commercial 3D printing systems currently available to fabricate items for these industries are limited to using either metal, ceramics, or thermoplastics.[5] This restricted material set limits widespread adoption and use of 3D printing to generate customizable and tunable structures for desired applications. Yield-stress fluids (extreme shear-thinning materials) that are direct writable using pneumatic extrusion are a nascent material class that is being explored to address the growing need for new inks for 3D printing.

The reported challenges in developing yield-stress fluid inks are to allow for the ability to both build structures and print small diameter filaments (l00 µm or smaller) with high shape-retention. A large variety of yield-stress fluids have been studied for use as inks for 3D and 4D printing (**Figure 1**a).[6] These materials may be organized according to the microstructural mechanism, such as particulate gels, polymer gel, jammed suspensions, emulsions, and foams, by which the yield-stress occurs.[7] While the range of reported yield stresses is very large (1 to over 1000 Pa), the resolution for the smallest reported nozzle diameter is ≈10 to 30 µm.[6] It has been noted that for applications that are limited by diffusion kinetics (e.g., biological,[8] actuation,[1] etc.), smaller filament diameters are required for the necessary mass-transport properties.

In most inks systems, reducing the filament diameter is only possible through decreasing the diameter of the nozzle used for printing. A major challenge in reducing the nozzle diameter is microstructural jamming through the tip. It has been shown that even with particles on the order of nanometers in diameter, large aggregates can form and result in clogging of the tip, with the additional complication of material drying at the tip.[6l] A possible approach to overcome this might be to reduce the loading/density of the material microstructure, however, this comes at the cost of a reduced yield stress.[6m] A previous attempt at this approach has resulted in materials that have too low of a yield stress or modulus to build large, open, self-supporting (i.e., gap-spanning) structures.[9] This trade-off creates a limitation on the types of 3D structures that may be built with available inks.

Extensible particle-free emulsions, which have not been previously studied, are here explored as an alternative yield-stress fluid to particle-stabilized or polymer-based gels. The dispersed phase of these emulsions acts as pseudoparticles that jam against each other in order to support a static load (Figure 1b). However, unlike hard colloidal nanoparticles, the emulsified droplets are able to deform to the shape of the tip and, if necessary, split to continue printing. The importance of extensional rheology has been established for extrusion processes such as injection molding and film formation,[10] but has not been investigated for direct-write 3D printing. It has been conjectured that a higher extensibility would stabilize a filament during extrusion, improving printing performance.[11] The ability to both deform/conform to the restrictions of the tip

Dr. B. M. Rauzan, Dr. S. E. Lehman, Prof. R. G. Nuzzo
Department of Chemistry
Frederick Seitz Materials Research Laboratory
University of Illinois at Urbana-Champaign
600 South Mathews Avenue, Urbana, IL 61801, USA
E-mail: r-nuzzo@illinois.edu
A. Z. Nelson, Prof. R. H. Ewoldt
Department of Mechanical Science and Engineering
Frederick Seitz Materials Research Laboratory
University of Illinois at Urbana-Champaign
1206 West Green Street, Urbana, IL 61801, USA
E-mail: ewoldt@illinois.edu

DOI: 10.1002/adfm.201707032

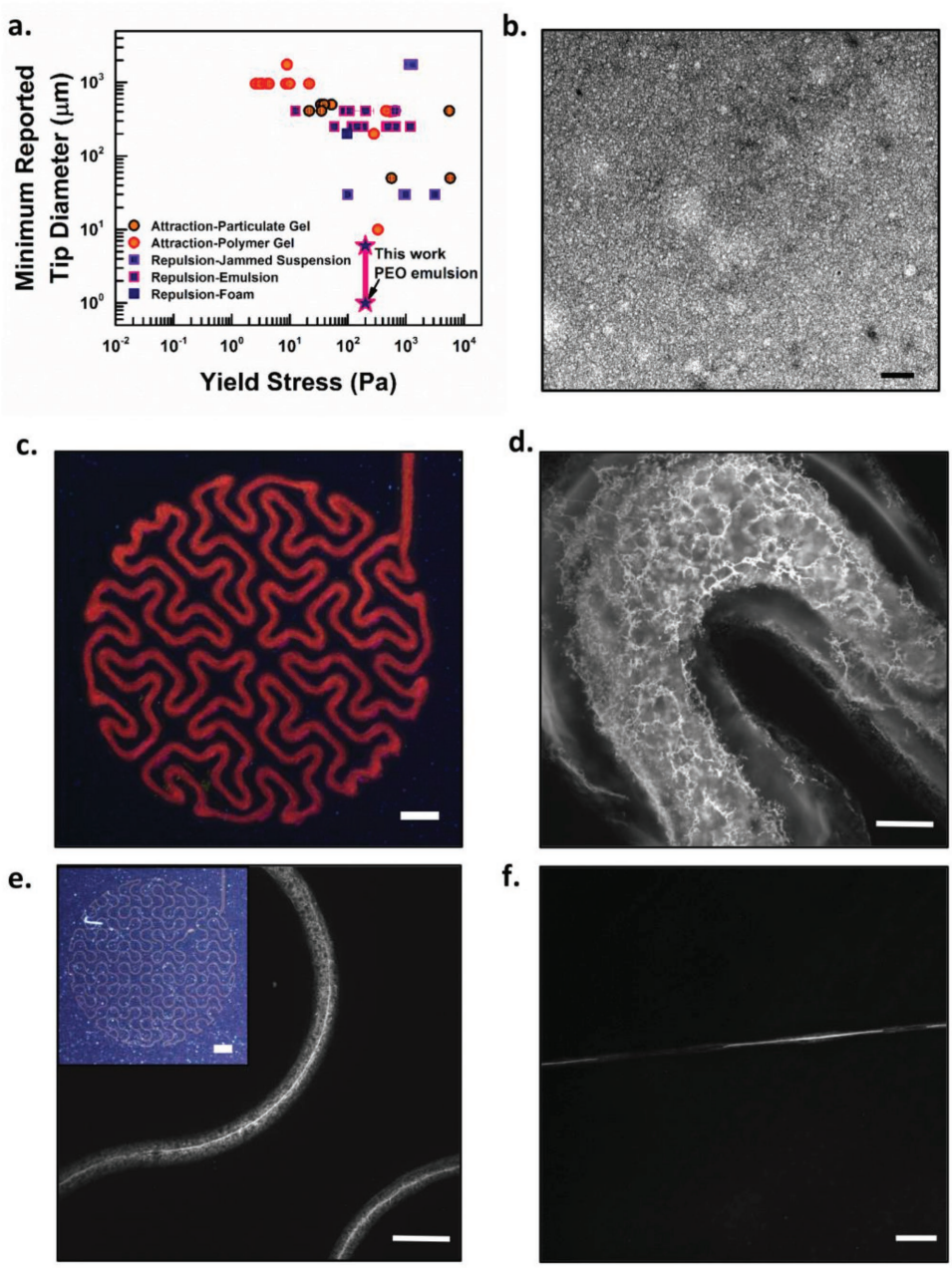

Figure 1. a) Minimum reported tip diameter as a function of yield stress for 3D printing yield-stress fluids organized by microstructure and yield-stress mechanism (attraction-particulate gel, attraction-polymer gel, repulsion-jammed suspension, repulsion-emulsion, repulsion-foam,[6] and PEO emulsion [reported in this work]. b) Transmitted brightfield microscopy of 8 M PEO emulsion with Congo Red. Scale bar: 50 μm. c) Macrofluorescence image of serpentine pattern of 8 M PEO emulsion with Rhodamine 6G printed with 100 μm diameter tip at 1 mm s^{-1}. Scale bar: 1 mm. d) Fluorescence microscopy of serpentine pattern of 8 M PEO emulsion with Congo Red printed with 100 μm diameter tip at 1 mm s^{-1}, scale bar: 50 μm. e) Fluorescence microscopy of serpentine pattern of 8 M PEO with Congo Red emulsion printed with 1 μm diameter tip at 1 mm s^{-1}. Scale bar: 100 μm. Inset: macrofluorescence image of serpentine pattern of 8 M PEO emulsion with Rhodamine 6G printed with 1 μm diameter tip at 1 mm s^{-1}. Scale bar: 1 mm. f) Fluorescence microscopy of line pattern of 8 M PEO emulsion with Congo Red printed with 1 μm diameter tip at 20 mm s^{-}. Scale bar: 50 μm.

geometry and diameter and exhibit high extensibility (500% or greater) introduces a novel class of inks for 3D printing.

In this work, we examine fabrication of particle-free silicone oil-in-water emulsions with a polymer additive, poly(ethylene oxide) (PEO), to form elastomeric structures. We use a printing-centric approach addressing three key areas of 3D printing performance (filament diameter, nozzle movement rate, and gap spanning). The molecular weight of PEO is varied to understand the relationship between microstructure, critical rheological properties (shear flow properties and extensibility—a property of yield-stress fluids that has only recently been acknowledged[7b]), and printing performance. Postprinting chemical and thermal annealing is performed on the particle-free emulsions to prepare elastomers, which have new

properties including mechanical buckling, and recovery from extreme compressive strain, which is not innate to the initial particle-free emulsions.

2. Results and Discussion

Particle-free emulsions are examined as an alternative microstructure for 3D printing inks to fabricate 3D structures and intricate small diameter filament patterns. In contrast to many of the reported inks in the literature, this novel material does not require incorporation of particles to achieve a sufficient yield stress for building (Figure 1a).[6] The yield stress (≈200 Pa in shear) is achieved with a microstructure that allows for extrusion of the material through a 1 µm diameter tip (Video S1, Supporting Information).

2.1. Fabrication of Particle-Free Emulsions and 3D Printed Filament Resolution

The emulsion is prepared as a stock particle-free silicone oil-in-water emulsion using sodium dodecyl sulfate (SDS) as a surfactant for the formation of micelles as well as stabilizing agent. The advantage of using a stock particle-free emulsion is that it provides a simple method for using a printing-centric approach to understand the impact on polymer additive on rheological properties and 3D printing performance of the material. PEO of different average molecular weights ranging from 400 K to 8 M g mol^{-1} (0.4–8 M) is incorporated into the stock-emulsions such that the final overall weight percent for all molecular weights is 0.1 wt% PEO. Transmitted brightfield microscopy of an 8 M PEO emulsion with the aqueous phase dyed with Congo Red (Figure 1b) shows a homogeneous emulsion with the dispersed phase of silicone oil droplets on the order of 10 µm in diameter.

PEO has been shown to form a complex with SDS micelles in surfactant solutions.[12] Dynamic light scattering and zeta potential measurements of aqueous solutions of SDS and 8 M PEO at the concentrations used in the emulsions are examined to determine interactions between the surfactant and the polymer additive in the emulsion materials. The hydrodynamic diameter for both SDS (Figure S1a, Supporting Information) and SDS with 8 M PEO (Figure S1d, Supporting Information) are polydisperse with the majority of micelles for SDS ≈1 nm and SDS with 8 M PEO ranging between 10 and 100 nm. The increase in hydrodynamic diameter is expected due to the interaction between SDS and PEO and formation of micelles, which is further confirmed by a decrease in the zeta potential for the SDS with 8 M PEO solution (Figure S1b,e, Supporting Information). The addition of PEO is proposed to interact with the electrical double layer present at the surface of the oil droplets (Figure S1c,f, Supporting Information) in a way that does not disrupt the native microstructure of the emulsion (Figure S2, Supporting Information).

The emulsion enables 3D printing to fabricate intricate patterns using multiple tip diameters. A fluorescence image of a serpentine pattern printed with an 8 M PEO emulsion dyed with Rhodamine 6G is shown in Figure 1c using a 100 µm diameter tip. The material displays excellent filament shape retention and is stable under normal conditions without filament distortion (dehydration or cracking). There is no apparent disruption to the microstructure of the emulsion evident when the serpentine pattern dyed with Congo Red is examined using fluorescence microscopy (Figure 1d). Due to an ability to easily deform the dispersed phase, the emulsion is able to be extruded through a 1 µm diameter tip,[5] which is not possible with commonly used inks due to microstructure jamming. Using the same serpentine pattern (Figure 1e inset), the emulsion was printed using a 1 µm diameter tip; both macroscopic (dyed with Rhodamine 6G) and microscopic (dyed with Congo Red) fluorescence images are shown in Figure 1e. In comparison to the sample printed with a 100 µm diameter tip, the reduction in the tip diameter and corresponding filament diameter allows for improved resolution of the features of the pattern as seen in the ability to resolve precise curvature of the pattern (Figure 1e), whereas the resolution of the curvature is compromised when the pattern is printed with a larger (100 µm) tip (Figure 1c). The ability to access smaller tip diameters as seen in the contrast between images is highly significant in expanding the capabilities to pattern intricate, complex patterns using 3D printing. It is also noted that reduction in filament diameter is not solely limited to reduction in nozzle size, but also can be accomplished through modification of nozzle movement rate. By increasing the nozzle movement rate to 20 mm s^{-1} and using the same conditions with a 1 µm tip used in Figure 1e, the filament diameter is reduced to ≈6 µm. The ability to use nozzle movement rate as an alternative method to regulate filament diameter will be discussed later.

At low nozzle movement rates (around 1 mm s^{-1}), die swell is observed, where the size of the extruded filament is greater than the diameter of the nozzle. The filaments printed through the 100 µm tip can swell to as large as 200 µm in diameter, while the filaments printed through the 1 µm diameter tip can swell to as large as 40 µm in diameter. The impacts of die swell can be mitigated by increasing the nozzle movement rate. Increasing the linear motion nozzle movement rate (20 mm s^{-1}) while maintaining the same tip and pressure conditions used in Figure 1e, the extruded filament of 8 M PEO achieves a filament diameter of 6.4 µm. Despite the continued presence of die swell in the filament, the smallest tip diameter this material may be extruded through and the final filament diameter are well below the limits seen with other yield-stress inks reported in the literature (Figure 1a). We emphasize that Figure 1a summarizes the reported minimum tip diameter of the cited works, and thus effects such as die swell in the filament are not accounted for. The 3D printing performance of these novel emulsions warrants careful examination of the relationship between microstructure, rheological properties, and printing performance.

2.2. Rheological Properties Enable 3D Printed Structures

The rheological properties of the emulsion and the impact of the PEO and its molecular weight were examined to explore the relationships that exist between rheology and printing performance. The specific performance criteria examined (vide infra)

in this work are filament resolution, maximum nozzle movement rate with continuous extrusion, and filament gap-spanning distance.

2.2.1. Shear Flow Properties

Shear flow properties of the emulsions were studied using bulk rheology. For the emulsion without PEO, the stock emulsion was diluted such that the fraction of oil to water was held constant for all samples. To within the reproducibility of characterization, there is no effect on the storage modulus (G') or loss modulus (G'') of the material due to changing the molecular weight of the PEO (**Figure 2**a). Trends in the average linear viscoelastic moduli are non-monotonic with the molecular weight of PEO, indicating that no clear functional dependency exists between these parameters. Steady shear flow behavior also is not significantly affected by the molecular weight of the PEO (Figure 2b), to within the range of the statistical significance of the measurements. At low applied shear-rates, the measured stresses approach a plateau, characteristic of the extreme shear-thinning of apparent yield-stress fluids (Figure S3, Supporting Information). The addition of polymer additives to particle-stabilized emulsions has been shown to result in changes to the shear flow properties, requiring optimization of the material for each polymer additive to restore the initial rheological properties.[6h] Such impacts are notably absent in the current ink system, where (as we will show) the

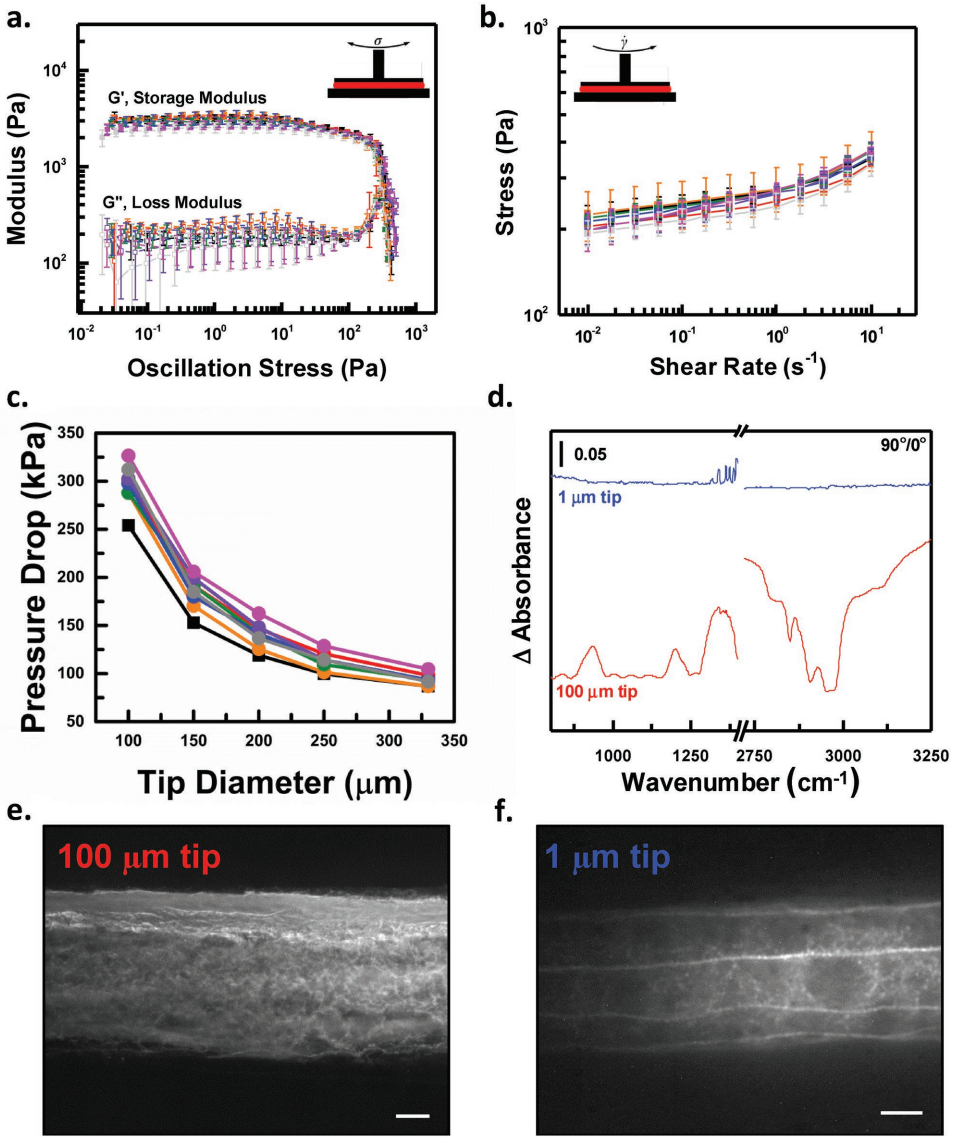

Figure 2. a) Storage modulus (G') and loss modulus (G'') as a function of oscillation stress. Error bars are from repeat measurements. No PEO (black), 400 K PEO (red), 600 K PEO (orange), 900 K PEO (green), 1 M PEO (blue), 4 M PEO (purple), 5 M PEO (pink), 8 M PEO (gray). Same for (a)–(c). b) Shear stress as a function of shear rate. c) Average pressure drop at the piston of syringe for extrusion at 1 mm s^{-1} as a function of tip diameter. d) Polarized FTIR of filament extruded at 1 mm s^{-1} from tip diameter of 100 μm (red) and 1 μm (blue), fluorescence microscopy of line pattern of 8 M PEO emulsion with Congo Red extruded at 1 mm s^{-1} from tip diameter of e) 100 μm; Scale bar: 50 μm. f) 1 μm; scale bar: 10 μm.

addition of the polymer additive provides a method to systematically vary only the extensional rheological properties and their consequent impact on 3D printing performance.

Tip flow properties were studied to determine how the polymer additive impacts the printing performance of the emulsion. To do so, the pressure drop at the piston of the syringe (P_{flow}) was determined during the pneumatic extrusion of a filament at a velocity of 1 mm s^{-1} at the given diameter of the nozzle (Figure 2c). Given that the pressure drop is independent of the amount of material in the syringe, we assume that the pressure drop at the piston of the syringe (P_{flow}) is approximately the same as that at the entrance to the nozzle (P_{tip}). The incorporation of PEO and increasing molecular weight of polymer (i.e., more extensible emulsion) does not hinder flow through the tip, which shows that shear rheology dominates the flow resistance in the nozzle. The printing of material through two different tip diameters was examined using polarization-dependent Fourier transform infrared (FTIR) spectroscopy measurements to determine differences in birefringence as might be present in the extruded filaments. The filament extruded from a 100 μm diameter tip is birefringent (Figure 2d), whereas the filament from a 1 μm diameter tip is not. The noted differences in optical properties are believed to be due to alignment of PEO domains due to tip confinement, and were further examined by fluorescence microscopy using filaments dyed with Congo Red. The material from the 100 μm diameter tip resembles the bulk 8 M PEO material (Figure 2e) and no difference is observed in microstructure for filaments extruded at this tip diameter without PEO (Figure S2b, Supporting Information). By contrast, the 8 M PEO material from the 1 μm diameter tip contains stripes, which are believed to be aqueous channels that extend continuously throughout the sample (Figure 2f). These channels are not present in the emulsion formed without PEO (Figure S2d, Supporting Information). As the molecular weight of PEO increases, the longer chains allow a higher extensibility of the material, an effect made visible as the drawing of thin filaments.

2.2.2. Extensional Rheology

Results from Filament Stretching Extensional Rheology measurements, at constant deformation rate ($\dot{\varepsilon} = 0.2\ s^{-1}$) are shown in **Figure 3**a. The presence and variations in the molecular weight of PEO do not cause any measurable differences in the extensional stress in the emulsion. Due to visual observations of thin filaments of material forming for high molecular weights of PEO, a very minute difference in the force response would be present at high strains. This minute difference is below the force measurement resolution of our experimental setup. Although there is no measurable difference in extensional stress, changes made in the molecular weight of the PEO and tip diameter do affect the ability of the emulsion to span a gap when printed (Figure 3b). Maximum gap spanning distances were determined by measuring the largest distance a printed filament is able to span without visual distortion (thinning) or sagging of the filament (Figure S4a,b, Supporting Information). High nozzle movement rates are desirable in general, and are more convenient for the assessment of gap-spanning properties. Thus, the linear motion nozzle movement rate was adjusted to 10 mm s^{-1}.

Gap spanning properties are evaluated at a range of nozzle diameters (100–330 μm). For tip diameters less than or equal to 200 μm, all of the emulsions are able to span a gap of 10 mm and there is minimal difference between all of the emulsions to gap span 10 mm with a 250 μm diameter tip (Figure 3b). Since the viscoelastic moduli and shear yield stress of the emulsions are comparable, it is not surprising that there is minimal difference in performance at these tip diameters. The gap spanning filaments are stable for greater than one month without any observed sagging or distortion. The ability to form intricate tubes interconnected with suspended filaments is highlighted in Figure 3c. Two noticeable features of the gap-spanning properties are: (1) the ability to fabricate a flying buttress-like structure with a filament that spans from a high point (structure) to a low point (substrate); and (2) an ability for gap-spanning filaments to support a second filament printed across to form a cross in the center of each tube. As noted with the spanning filaments, the tubes are stable for greater than one month without observed distortion to the structure. A more apparent difference in ability to gap span occurs when using a 330 μm diameter tip. With this tip diameter, only 4 M, 5 M, and 8 M molecular weight PEO are able to span gap distances greater than 6 mm. Since these materials are not distinguishable from the lower molecular weight materials in terms of shear rheological properties, there must be a component of the extensional behavior that allows for molecular chain elongation and reinforcement of the emulsion to span large gaps using this large tip diameter.

Extensional failure strain is the final rheological property examined to understand the role of chain elongation in printing performance. The percent strain-to-break for the emulsions was measured as a function of the molecular weight of the PEO (Figure 3c). Macroscale images of filaments, ≈100 μm, (shown in Figure 3) allow visualization of the high extensibility (greater than 500%) of emulsions formed with 4 M, 5 M, and 8 M molecular weight PEO (Video S2, Supporting Information). Emulsions with extensional failure strain greater than or equal to 500% correlate directly with gap-spanning capabilities seen at large tip diameters.

Increased extensibility creates an interplay between pneumatic and drag extrusion of the inks. For most inks, increasing the nozzle movement rate for a structure requires an increase in the pressure applied to maintain a constant flow of material through the tip. Highly extensible materials maintain a tensile stress that increases with nozzle movement rate to supplement the pressure-driven flow. This allows nozzle movement rate to be used to regulate filament diameter and produce filaments with a diameter smaller than the extrusion tip diameter.[13]

The maximum nozzle movement rate of each emulsion was determined at the pressure that produces a linear rate of 1 mm s^{-1} through a 100 μm diameter tip. For each sample, maximum nozzle movement rate is determined by the rate at which the material can be extruded continuously to complete a defined line pattern. The emulsions with extensional failure strains of 500% or greater are able to print continuous filaments at 20 mm s^{-1} (**Figure 4**c; Video S3, Supporting Information). By contrast, samples with low extensional failure strain, such as the emulsion without PEO, are not able to print at these high nozzle movement rates. When low extensibility materials are

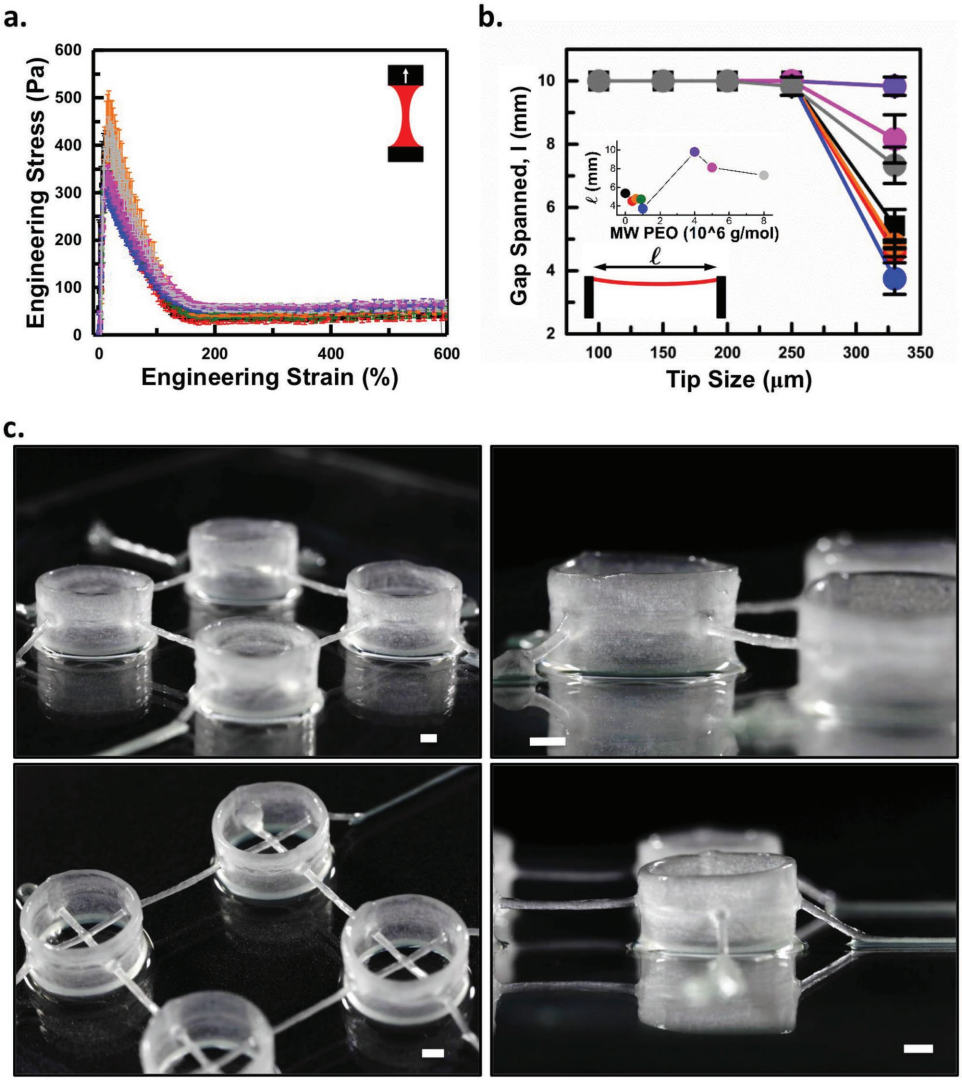

Figure 3. a) Extensional filament stretching, error bars are from repeat measurements. No PEO (black), 400 K PEO (red), 600 K PEO (orange), 900 K PEO (green), 1 M PEO (blue), 4 M PEO (purple), 5 M PEO (pink), 8 M PEO (gray). Same for (a)–(b). b) Gap spanned as a function of tip size. Inset shows gap spanned as a function of molecular weight of PEO for the largest diameter tip with error bars omitted in inset for clarity. c) Macroimage of tubes interconnected with suspended filaments of 8 M PEO emulsion printed with 100 μm diameter tip and exposed to silicon tetrachloride vapor chemical anneal, scale bar: 1 mm.

printed, instead of continuous filaments, elongated discrete dots of material are formed, with the spacing between the dots dependent on the nozzle movement rate (Figure S5, Supporting Information). Printing materials with high extensional failure strain, such as the 8 M PEO emulsion shown in Figure 4d, results in the ability to decrease filament diameter by counteracting die swell. The high extensibility of the material allows for fast movement rates to be used to draw filaments of the material when printing. The ability to use extensional failure strain to moderate die swell behavior is a generalizable approach, which can easily be applied in general to the 3D printing of other inks by incorporating additives, such as high molecular weight PEO. When the PEO emulsion is printed at a rate of 1 mm s^{-1} using a 100 μm diameter tip, the diameter of the filament is ≈180 μm. Increasing the nozzle movement rate to 20 mm s^{-1} produces a filament that is 100 μm in width, the same diameter as the tip, and exhibits no die swell. While the maximum nozzle movement rate for our printer setup is limited to 20 mm s^{-1}, we expect the high extensibility of these materials would enable printing of filaments that are smaller than the tip diameter if higher nozzle movement rates are accessible. This provides an opportunity for effecting greater control over filament diameter by using nozzle diameter coupled with nozzle movement rate to fine tune filament diameter and access small diameter filaments without the limitation of using small diameter nozzles as are required with more conventional materials for 3D printing.

2.3. Synthesis of 3D Printed Mechanically Robust Elastomers

3D printing emulsions opens the possibilities for postprinting transformations of materials chemistries to introduce new

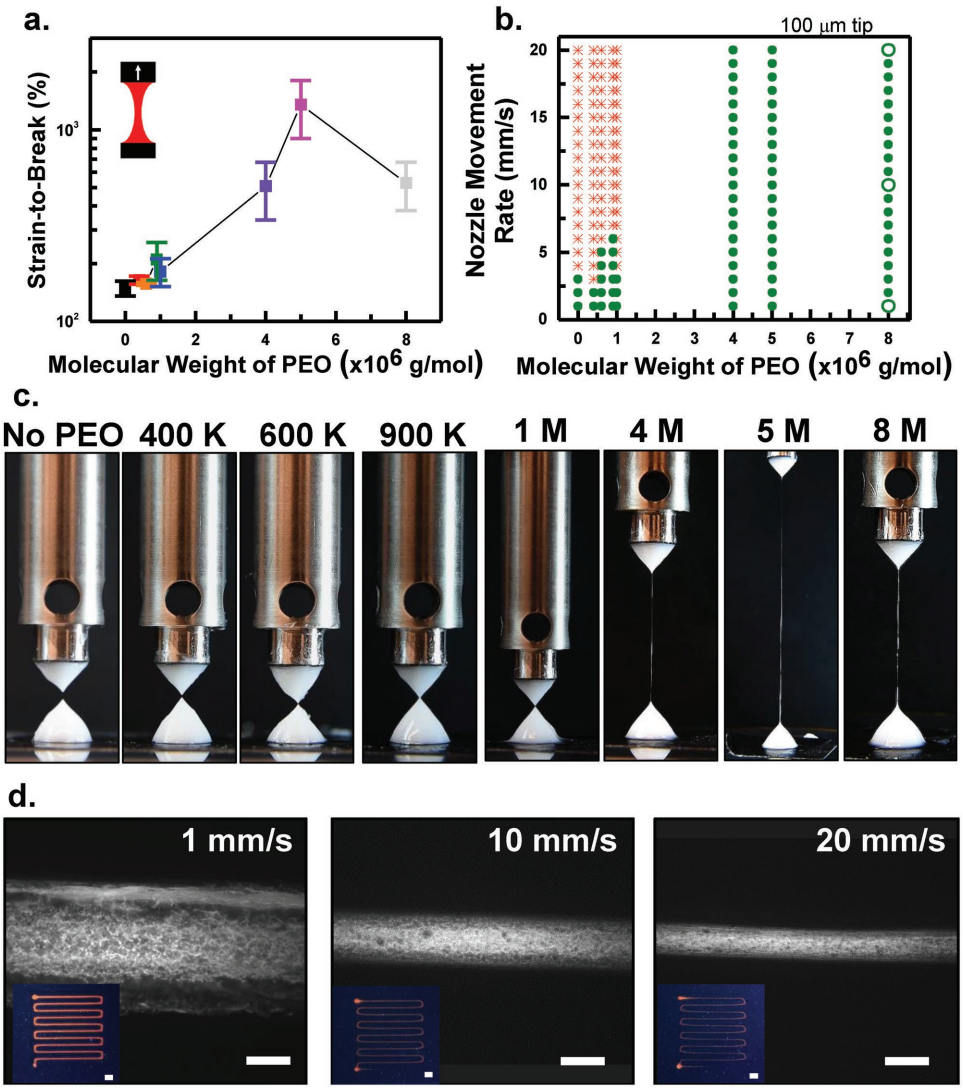

Figure 4. a) Extensional strain-to-break (%) as a function of molecular weight of PEO. b) Maximum nozzle movement rate for continuous extrusion (green symbol) of filament as a function of molecular weight of PEO, see Supporting Information for images of discontinuous extrusion (red symbol). c) Macroimages at maximum filament extension with increasing molecular weight of PEO. The diameter of the upper geometry is 8 mm in all images. d) Fluorescence microscopy of line pattern of 8 M PEO emulsion with Congo Red printed with 100 μm diameter tip at 1, 10, and 20 mm s^{-1} (open data points in (b)). Scale bar: 100 μm. Inset: macrofluorescence image of line patterns. Scale bar: 1 mm.

properties and/or structures into the printed structures that are not innate to the native material. These posttransformation chemistries include, but are not limited to, formation of a metal oxide structures,[14] polymerization,[15] and growth of nanoparticles.[16] We present a two-step approach, chemical annealing followed by thermal annealing (**Figure 5**a), to convert the emulsion into an elastomer that is stable in solvent (organic and aqueous) and mechanically tough and resilient, two properties not native to the emulsions as present directly after printing.

For this conversion of emulsion to an elastomer, we take advantage of the water in the continuous phase of the printed structure to react with gaseous silicon tetrachloride, which generates a thin silica shell on the exterior of the structure. This silica shell provides only a minimal enhancement of mechanical stability, and the structure is able to be easily compressed. Doing so between ZnSe plates for FTIR studies, we found that there is only a slight peak shape change seen in the Si–O–Si (1000 to 1100 cm^{-1}) region after chemical annealing (Figure 5b), which is attributed to the formation of silica. The peak shape for the Si–O–Si region remains broad, which resembles what would be expected for stretching vibrations for a predominantly silicone composition and not silica.[17] This further confirms that the silica formed during chemical annealing is only a thin shell. As an additional control, after chemical annealing but before thermal annealing, the sample is irreversibly compressed when 50 g weight is applied to the glass coverslip on top of the structure (Figure S8 and Video S6, Supporting Information).

Thermogravimetric analysis (TGA) of the emulsion and chemical annealed emulsion also confirms formation of silica as evidenced by the residual mass for the sample that had been chemically treated. This is compared to the initial emulsion in

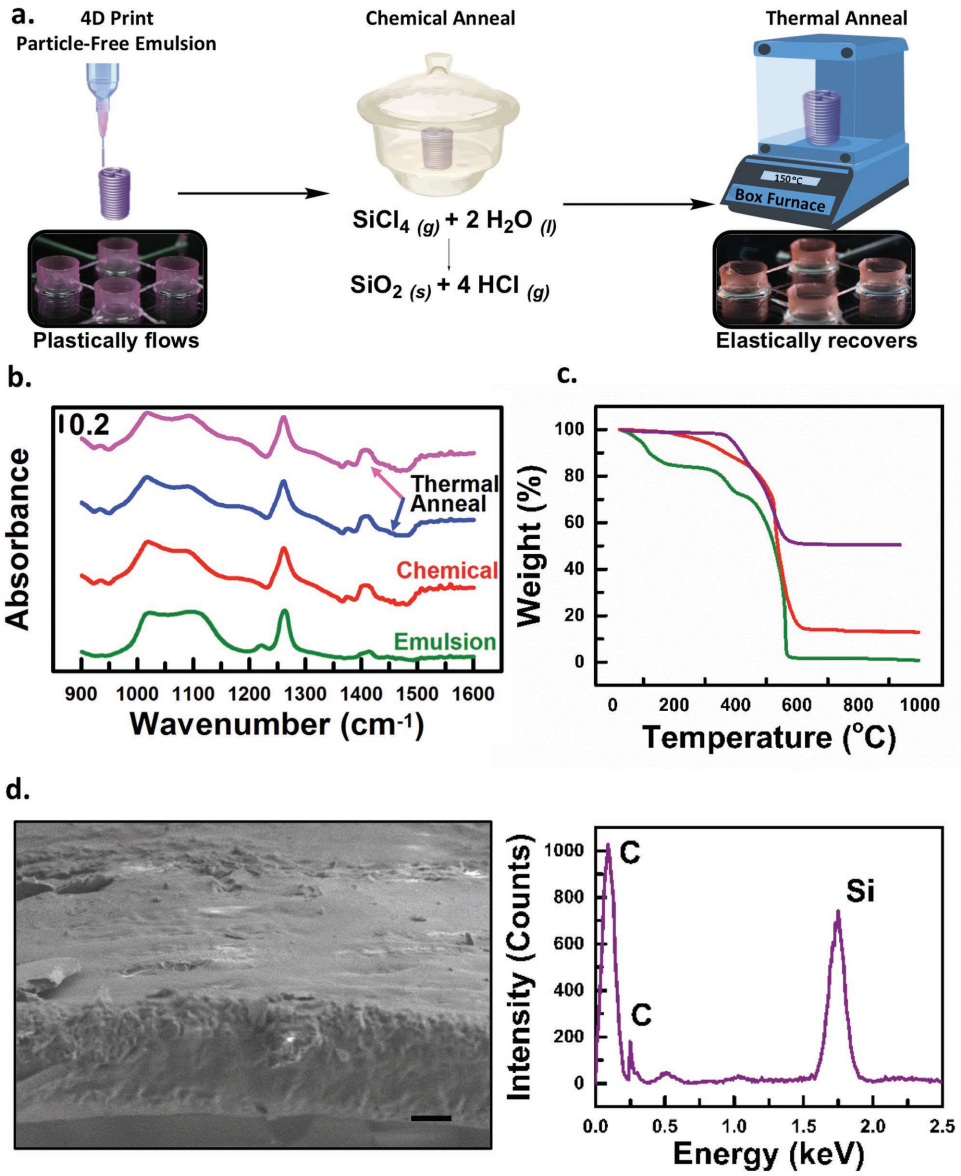

Figure 5. a) Two-step preparation process, chemical and thermal anneal, of elastomer from printed particle-free emulsion. b) FTIR of printed particle-free emulsion as printed (green), after chemical anneal (red), after annealing at 80 °C for 30 min (blue), after annealing at 80 °C for 30 min and 150 °C for 1 h (pink). c) TGA of particle-free emulsion (green), after chemical anneal (red), after chemical and thermal anneal (purple). d) SEM and EDX of thermally annealed tube coated with a 2.5 nm layer of a 60:40 Au/Pd alloy. Scale bar: 20 µm.

which total mass loss is observed only once the temperature exceeds ≈600 °C. The mass loss from 0 to 200 °C is attributed to water and out-gassing of the material (as has been reported previously in the literature).[18]

The chemically annealed emulsion structures can be subsequently transformed via thermal processing. To do so, the structures bearing a thin silica shell are thermally annealed through a multistep temperature ramp from room temperature to 292 °C. This treatment leads to the thermal polymerization of the silicone oil used to formulate the ink emulsion. This silicone oil, used unmodified from the Sigma-Aldrich source, is polydisperse (gel permeation chromatography (GPC) analysis (THF) M_w = 37.98 kDa, PDI = 1.56; M_w = 1.31 kDa, PDI = 1.02; M_w = 0.83 kDa, PDI 1.01, Figure S6a, Supporting Information) and contains trace amounts of copper as evidenced by X-ray fluorescence (XRF) (Figure S6b, Supporting Information), as well as silicon hydride (peak at 2050 cm^{-1})[19] and silicon hydroxide (peaks at 3600–3800 cm^{-1})[20] moieties as evidenced by FTIR (Figure S6c, Supporting Information). The trace amounts of copper are believed to be a residual impurity resulting from the process used in the production of the silicone oil.[21] Since the silicone oil contains reactive functional groups (hydride and hydroxide), the presence of the copper leads to a thermally activated one-part condensation silicone cure to form an elastomer (a property also seen in control experiments using only bulk samples of the silicone oil).

The silica shell is crucial to provide mechanical stability to the structure during the thermal annealing process. Without the silica shell, the structure collapses and results in polymerized

silicones without shape retention. FTIR of the samples, performed during the first and second temperature ramp, show no major chemical changes occur as compared to the chemical annealed sample (Figure 5b). The printed structures in this case, however, are mechanically robust and able to recover from significant degrees of deformation (see below). Taken together, the data suggest that the two-stage temperature ramp of the thermal annealing cycle leads to the evolution of residual water from the structure and coalescing of the dispersed phase, the silicone oil, to form a continuous silicone matrix encapsulated in silica. How the low wt% of SDS and PEO that remain are dispersed in the final silicone structure is not fully understood based on the data currently available. We simply note that their presence seems to have little impact on the mechanical properties of the final structures, a point discussed in greater detail in the section that follows.

After the final thermal annealing step, the resulting material is an elastomer that is stable when exposed to both organic and aqueous solvents, a property not native to the emulsion. Thermogravimetric analysis of the elastomer shows increased thermal stability with minimal mass loss at temperatures less than 380 °C (Figure 5c). This is comparable to reports in the literature, which show the onset of thermal breakdown of polydimethylsiloxane (PDMS) to be around 350 °C.[18] Polymerization of the dispersed silicone oil through thermal annealing is further confirmed by scanning electron microscopy with energy dispersive X-ray spectroscopy (SEM/EDX) (Figure 5d) showing a smooth continuous surface composed of silicon and carbon.

The ability to introduce enhanced mechanical stability to the structure in response to an external force is critical for the structure to robustly perform in a multitude of applications such as might be required for a soft actuator. The modification of the mechanical performance of the structure through postprinting transformation also highlights the fundamental principles and novelty of 3D printing to transform a 3D printed structure. The Young's modulus of the thermal annealed sample was measured and fit using the Oliver and Pharr model (**Figure 6**a). The Young's modulus of the material is 1.1 ± 0.4 MPa, which is comparable to the elastic modulus of PDMS (0.57–3.7 MPa)[22] and a factor of up to 500 times greater than the linear viscoelastic modulus of the printed emulsion (2–3 kPa). With the increase in the modulus, printed and processed tubes interconnected with suspended filaments are able to support a glass coverslip with a 10 g weight without any visible deformation (Figure 6b; Video S4, Supporting Information). Further, the material exhibits reversible extreme buckling and elastic recovery (recovers $\varepsilon_{true} \approx -1.6$) compared to the printed emulsion which plastically flows at a yield strain $\gamma_y \approx 0.3$ (Figure S7, Supporting Information). The ability for the sample to undergo extreme buckling and compressive strain from a 50 g weight with a full recovery is shown in Figure 6c and Video S5 (Supporting Information). The drastic modification and enhancement to the mechanical properties of the material are due to the thermal polymerization of the dispersed silicone phase of the sample.

3. Conclusion

Particle-free emulsions with poly(ethylene oxide) are developed as an alternative ink for the production of elastomeric structures. Due to the ease of deformation of the silicone oil in the dispersed phase the material is able to be extruded through a 1 µm diameter tip to create intricate patterns. The shear flow properties are not significantly affected by the presence or molecular weight of the poly(ethylene oxide). Increasing the molecular weight of poly(ethylene oxide) drastically changes the extensibility of the material. Emulsions with extensional failure strain of 500% or greater allow for gap spanning and increased rate of printing to both reduce die swell and control filament diameter size. Postprinting transformation through a two-step annealing process, chemical and thermal, allows for fabrication of 3D printed elastomers. The elastomer is able to buckle and recover from extreme compression strain (compress to ≈20% original height of structure) with no observable damage to the structure. Particle-free emulsions with high extensibility are presented as a novel and exemplary class of yield-stress fluids to 3D print elastomers.

4. Experimental Section

Materials: SDS, silicone oil with a viscosity of 1000 cSt (at 25 °C), poly(ethylene oxide) (average M_v 400 000, 600 000, ≈900 000, ≈1 000 000, ≈4 000 000, ≈8 000 000 powder), Congo Red, Rhodamine 6G, methylene blue (1.5 g/100 mL), silicone tetrachloride (99%), hexanes (ACS Reagent grade), 200 proof ethyl alcohol, and isopropyl alcohol (ACS Reagent grade) were purchased from Sigma-Aldrich and used without modification.

Methods—Particle-Free Stock Emulsion: Silicone oil was homogenized with a mixture of SDS in deionized water to produce the stock oil-in-water emulsions. The overall weight-percentages for the stock emulsions were 90 wt% oil, 3.34 wt% SDS, and 6.66 wt% water. All components were added to a beaker and homogenized at 5000 rpm for 5 min using an IKA T-18 homogenizer with an S18N-19G dispersing element attachment.

Particle-Free Emulsion with Poly(ethylene oxide) Inks: Poly(ethylene oxide) solutions of each M_v were prepared by dispersing the appropriate powder in a small amount of ethyl alcohol (cosolvent) at 30 °C and 200 rpm using a magnetic stirrer; deionized water was then quickly added to result in 1 wt% PEO solutions. Using measurements of intrinsic viscosity for PEO solutions reported by Kawaguchi et al. in dL g^{-1},[23] the overlap concentration (c*) was estimated as the inverse of the intrinsic viscosity assuming a density for PEO of 1.21 g mL^{-1}. The range of concentration normalized by overlap concentration for the PEO solutions was from 0.04 to 20. Each ink was produced by hand-mixing the stock emulsion and a PEO solution in a 9-to-1 weight ratio. A 0 wt% PEO (deionized water only) ink was produced as a control material. For imaging, PEO solutions were prepared with Congo red (0.6 wt%), Rhodamine 6G (0.09 wt%), or methylene blue (0.1 wt%). All inks were centrifuged at 3000 rpm for 5 min using a Thermo Scientific CL2 centrifuge before use or characterization.

Rheological Characterization—Shear Rheology: Rheological characterization of steady flow and linear viscoelastic properties was performed on rotational rheometers (combined motor/transducer instruments, TA Instruments DHR-3 or AR-G2) using a parallel-plate geometry with a diameter of 20 mm and Peltier temperature control. Adhesive-backed 600 grit silicon carbide sandpaper was used to prevent slip. Materials were tested at multiple gaps to verify the absence of slip.[24] During characterization, the gap was continuously varied to maintain a normal force of 0 ± 0.1 N and avoid edge fracture. For steady flow behavior, a range of shear rates were applied from low-to-high and the apparent steady stress was recorded. These data were fit to the Herschel–Bulkley model to obtain a yield-stress value of ≈200 Pa. For nonlinear viscoelasticity, an increasing oscillatory strain amplitude was applied at a frequency of 10 rad s^{-1} until failure of the material. Little frequency dependence was observed for any of the materials across the

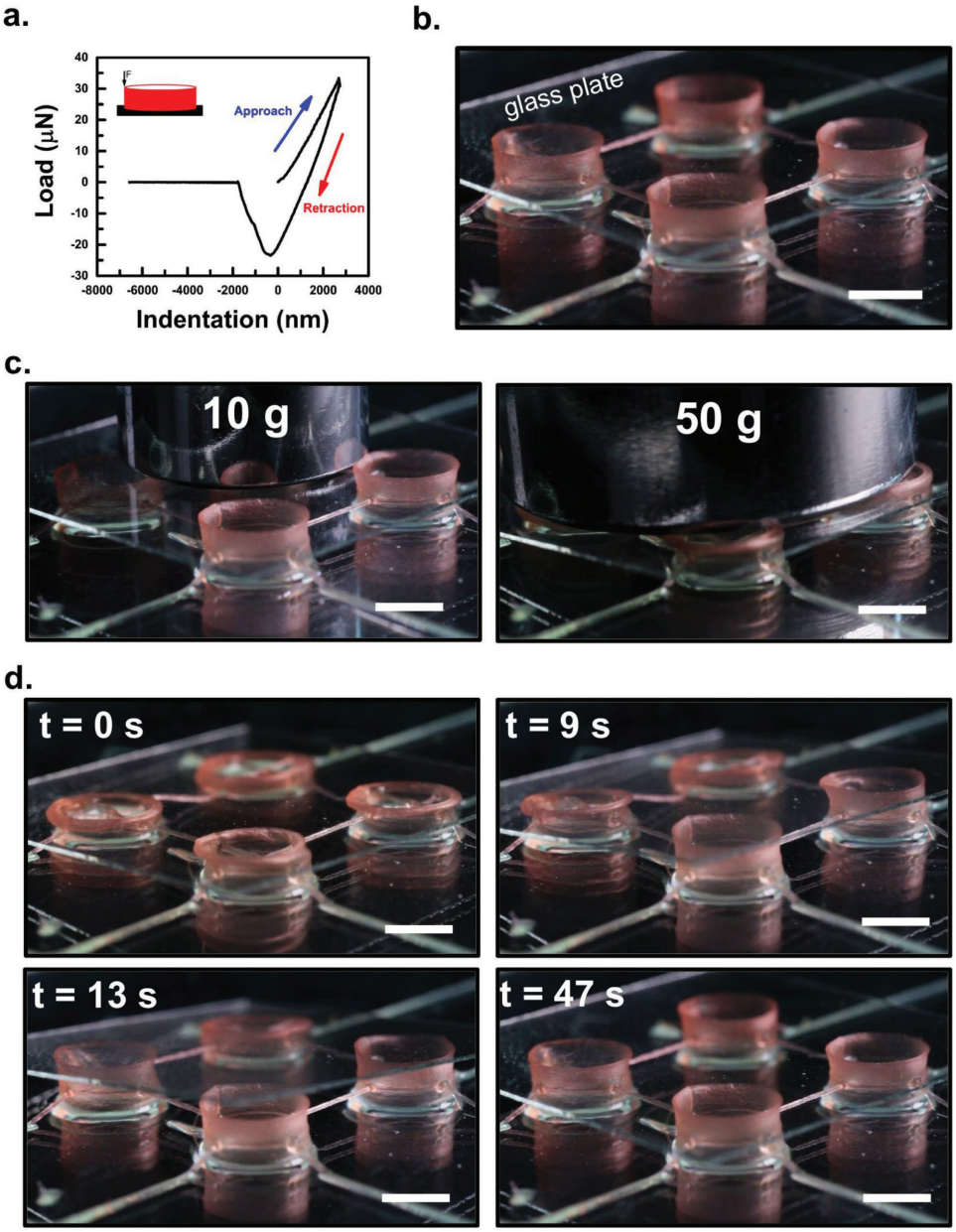

Figure 6. a) Force curve of thermally annealed particle-free emulsion obtained using a nanoindenter on the edge of a thermally annealed tube. Macroimage of tubes interconnected with suspended filaments of thermally annealed 8 M PEO emulsion with Rhodamine 6G. Scale bar: 5 mm. b) With glass coverslip, c) with glass coverslip supporting a 10 g weight and buckling under a 50 g weight, and d) time sequence of recovery after buckling.

range of 0.1 to 30 rad s^{-1}. All experiments were performed at 25 °C and replicated thrice to obtain error bars.

Extensional Rheology: Characterization for force-extension behavior and extensional strain-to-break were performed using a filament-stretching mode on a TA Instruments ARES-G2 rheometer (separated rotational motor/transducer, combined axial motor/transducer) as described by Nelson et al.[7b] For the filament-stretching experiments, a parallel-plate geometry with a radius of $R_0 = 4$ mm and advanced Peltier system bottom plate were used. The samples were loaded at a gap of $H_0 = 4$ mm, resulting in an aspect ratio of $\Lambda_0 = H_0/R_0 = 1$. A constant true strain rate, $\dot{\mathcal{E}} = 0.2\ s^{-1}$, was applied and engineering stress was recorded. Videos of the Supporting Information were taken during all extensional tests, and images were correlated with the measured load and displacement to determine the extensional strain-to-break. All experiments were performed at 25 °C and replicated thrice to obtain error bars.

3D Printing: A custom-built 3D printer consisting of a pneumatic extruder (Ultimus V and HPx High-Pressure Dispensing Tool, Nordson EFD) mounted to an X, Y, Z motion controller (AGS-1000, Aerotech Inc., Pittsburgh, PA) was used. All inks were loaded into syringes with either stainless steel, straight tip (tip diameter range of 330–100 μm, Nordson EFD) or glass capillary, tapered tip (1 μm, World Precision Instruments, LLC), and the syringes were loaded into the pneumatic extruder. Structures were printed on either glass slides or coverslips.

Code Availability: G-code for all structures printed in Figures 1, 3, 4, and 6 is available upon request.

Pressure Drop: For each stainless steel, straight tip diameter, pressure was applied to the system for 10 s using the pneumatic extruder from

the 3D printer described previously. If no extrusion of material was observed, the pressure was increased by 0.1 psi. The pressure (P_{flow}) was increased until sufficient pressure was applied for extrusion of a filament of the material with the diameter of the tip at a linear flow rate of 1 mm s^{-1}. The measured pressure (P_{flow}) was measured as the pressure drop at the syringe piston and assumed to be the same pressure at the entrance to the nozzle (P_{tip}).

Nozzle Movement Rate: A stainless steel, straight tip (100 µm diameter) was used to determine the maximum nozzle movement rate for extrusion of a uniform filament. For all nozzle movement rates, the pressure applied to the syringe was the pressure determined during the pressure drop (see prior Methods section) for extruding the ink from a 100 µm diameter tip at a linear flow rate of 1 mm s^{-1}. The nozzle movement rate was increased in 1 mm s^{-1} increments to a maximum of 20 mm s^{-1} to determine the maximum nozzle movement rate.

Gap Spanning: For each stainless steel, straight tip diameter, pressure (5× pressure determined for a linear flow rate of 1 mm s^{-1}) was applied to the system and the material was extruded across a template with different gap sizes ranging from 0.25 to 10 mm at a nozzle movement rate of 10 mm s^{-1}. The material was determined to span a gap if there was no sagging or change in the filament diameter (filament thinning) over the gap distance upon qualitative optical inspection.

Elastomer Synthesis: 3D printed emulsion structures were placed in a desiccator connected with a three-way valve to a three-necked 100 mL round bottom flask. The desiccator was sealed and the entire system was evacuated using a laboratory vacuum pump. The valve to the round bottom flask was closed and silicon tetrachloride (5–15 mL, dependent on the number and size of structure) was added via syringe. The valve was opened and heated via a heat gun for 1 min to allow the silicon tetrachloride vapor to diffuse into the desiccator. The samples reacted with silicon tetrachloride vapor overnight. The samples were then removed from the desiccator and thermally annealed in a box furnace (73 °C for 30 min, 143 °C for 1 h, and 292 °C for 1 h). The samples were allowed to cool to room temperature and then washed sequentially with hexanes, isopropanol, and water.

Elastomer Characterization—XRF: A Shimadzu EDX-700 System (100 µA, 50 kV, beam size diameter of 1 mm) with a rhodium source and purged with helium was used for XRF measurements. An elemental survey was performed to determine trace metals in the samples.

GPC: A Waters1515 Isocratic HPLC pump equipped with a Waters (2998) Photodiode Array Detector, a Waters (2414) Refractive Index Detector, a Waters (2707) 96-well autosampler in THF at 30 °C, and a series of 4 Waters HR Styragel columns (7.8 × 300 mm, HR1, HR3, HR4, and HR5) was used for GPC measurements. Monodisperse polystyrene standards were used to calibrate the instrument.

FTIR: A FTS-6000 FTIR spectrometer (Bio-Rad, Cambridge, MA) with DTGS detector, KBr beam splitter, and ceramic source was used for all IR measurements. Spectra were collected using a spectral resolution of 4 cm^{-1} with a modulation of 5 kHz and a 1.2 kHz low pass filter. Single beam spectra were coadded (64 scans) and referenced to ZnSe. For polarized measurements, a KRS-5 Au wire grid polarizer was used. Single-beam spectra were transformed using Varian Resolutions Pro software.

TGA: A TGA (TA Instruments) was used for all measurements. All samples were analyzed in a nitrogen environment. Two different heating cycles were performed: (1) linear temperature ramp (10 °C min^{-1}) from room temperature to 700 °C and (2) ramp (5 °C min^{-1}) to 73 °C, hold for 30 min, ramp (5 °C min^{-1}) to 143 °C, hold for 1 h, ramp (10 °C min^{-1}) to 292 °C, hold for 1 h. Data were analyzed using TA Instrumental Analysis software.

SEM with EDX: An Emitech K575 sputter coater was used to apply a nonconductive 2.5 nm layer of a 60:40 Au/Pd alloy (applied current of 20 mA for 10 s, deposition rate of 2.5 Å s^{-1}) coating to the samples prior to imaging. Coated samples were immobilized onto a metallic sample exchanger using carbon tape and loaded into a Hitachi S4700 scanning electron microscope. The samples were imaged using an extracting voltage of 10 kV and a beam current of 10 µA. EDX was carried out using an Oxford instrument on imaged sections of the sample via 15 keV X-ray irradiation and data were accumulated for 300 s to give the resulting spectra using Iridium software.

Modulus Characterization: A Piuma Nanoindenter was used for all measurements. Indentations were performed with a probe (tip radius of 9.0 µm, stiffness of E_{eff} = 44 N m^{-1}, Poisson's ratio approximately of ν = 0.5, calibration factor of 1.3) over 10 µm relative displacement and overall indentation time of 6 s. Piuma Dataviewer Version 1.0 by Optics was used to analyze the data and the retraction portion of the indentation curve was fit to the Oliver and Pharr model (lower load limit was set to 65% of the maximum load (P_{max}) and upper load limit set to 85% of the maximum load (P_{max})).

Imaging: Microstructural observations were made using an Olympus IX71 inverted fluorescence microscope with a GS3-U3-23S6M-C Point Grey CCD camera and a mercury vapor lamp light source. Images were recorded with a 10× UPlanSApO or 63× Zeiss LD Plan NEO air immersion objective lenses at various locations across samples. Macro images were taken with a Canon EOS 5D Mark II DSLR camera with an MP-E 65 mm lens and a UVP Black-Ray B-100AP UV Lamp.

Data Analysis and Fitting: Figure 1a is generated from digitizing literature data[6] of steady shear flow or large-amplitude oscillatory shear using WebPlotDigitizer on Chrome. Using OriginPro 2016, digitized steady shear data of stress versus strain-rate was fit to the Herschel–Bulkley model in applicable regions to obtain the shear yield stress. If necessary, a parallel-plate correction was performed prior to fitting.[25] All fits had an adjusted R^2 value of at least 0.90. For large-amplitude oscillatory shear data, the stress at the crossover of G' and G'' was taken as the yield stress. The minimum tip diameter was taken as reported. Microstructure type was taken as reported or categorized based on the authors' best judgment of the dominant microstructural yield-stress mechanism of the reported material.[7a] Note that many of these materials are complex multicomponent systems and the listed category is for the presumed "dominant" yield-stress mechanism.

Supporting Information

Supporting Information is available from the Wiley Online Library or from the author.

Acknowledgements

B.M.R. and A.Z.N. contributed equally to this work. The authors gratefully thank U.S. Department of Energy, Office of Science, Basic Energy Science (DE-FG02-07ER46741) for the support of the materials development efforts of this work. Printing capabilities used in this research were developed and are maintained by the Army Research Office MURI (W911NF-17-1-0351). Experiments were carried out in part in the Frederick Seitz Materials Research Laboratory Central Research Facilities, University of Illinois. The authors thank Abigail Halmes for assistance with GPC measurements, Lou Ann Miller for assistance with TGA measurements, and Natalie Becerra-Stasiewicz for assistance with modulus and XRF measurements. The authors thank Danrong Li for assistance with data analysis and fitting for Figure 1a. The authors thank Dr. Joselle McCracken and Dr. Yu Hao Liu for assistance with designing G-code for 3D printing.

Conflict of Interest

The authors declare no conflict of interest.

Keywords

3D printing, elastomers, emulsions, extensibility, rheology

Received: December 4, 2017
Revised: February 22, 2018
Published online: March 30, 2018

[1] A. S. Gladman, E. A. Matsumoto, R. G. Nuzzo, L. Mahadevan, J. A. Lewis, *Nat. Mater.* **2016**, *15*, 413.
[2] M. Wehner, R. L. Truby, D. J. Fitzgerald, B. Mosadegh, G. M. Whitesides, J. A. Lewis, R. J. Wood, *Nature* **2016**, *536*, 451.
[3] S. J. Song, J. Choi, Y. D. Park, S. Hong, J. J. Lee, C. B. Ahn, H. Choi, K. Sun, *Artif. Organs* **2011**, *35*, 1132.
[4] A. D. Valentine, T. A. Busbee, J. W. Boley, J. R. Raney, A. Chortos, A. Kotikian, J. D. Berrigan, M. F. Durstock, J. A. Lewis, *Adv. Mater.* **2017**, *29*, 1703817.
[5] Y. Gai, J. W. Khor, S. K. Tang, *Lab Chip* **2016**, *16*, 3058.
[6] a) E. Feilden, E. G.-T. Blanca, F. Giuliani, E. Saiz, L. Vandeperre, *J. Eur. Ceram. Soc.* **2016**, *36*, 2525; b) J. Zhong, G.-X. Zhou, P.-G. He, Z.-H. Yang, D.-C. Jia, *Carbon* **2017**, *117*, 421; c) Y. Shao, D. Chaussy, P. Grosseau, D. Beneventi, *Ind. Eng. Chem. Res.* **2015**, *54*, 10575; d) Y. Zhang, J. R. Evans, *J. Colloid Interface Sci.* **2013**, *395*, 11; e) K. Sun, T. S. Wei, B. Y. Ahn, J. Y. Seo, S. J. Dillon, J. A. Lewis, *Adv. Mater.* **2013**, *25*, 4539; f) K. Cai, J. Sun, Q. Li, R. Wang, B. Li, J. Zhou, *Appl. Phys. A* **2010**, *102*, 501; g) J. T. Muth, D. M. Vogt, R. L. Truby, Y. Menguc, D. B. Kolesky, R. J. Wood, J. A. Lewis, *Adv. Mater.* **2014**, *26*, 6307; h) C. Minas, D. Carnelli, E. Tervoort, A. R. Studart, *Adv. Mater.* **2016**, *28*, 9993; i) M. R. Sommer, L. Alison, C. Minas, E. Tervoort, P. A. Ruhs, A. R. Studart, *Soft Matter* **2017**, *13*, 1794; j) J. T. Muth, P. G. Dixon, L. Woish, L. J. Gibson, J. A. Lewis, *Proc. Natl. Acad. Sci. USA* **2017**, *114*, 1832; k) G. Siqueira, D. Kokkinis, R. Libanori, M. K. Hausmann, A. S. Gladman, A. Neels, P. Tingaut, T. Zimmermann, J. A. Lewis, A. R. Studart, *Adv. Funct. Mater.* **2017**, *27*, 1604619; l) J. O. Hardin, T. J. Ober, A. D. Valentine, J. A. Lewis, *Adv. Mater.* **2015**, *27*, 3279; m) J. N. Hanson Shepherd, S. T. Parker, R. F. Shepherd, M. U. Gillette, J. A. Lewis, R. G. Nuzzo, *Adv. Funct. Mater.* **2011**, *21*, 47.
[7] a) A. Z. Nelson, R. H. Ewoldt, *Soft Matter* **2017**, *13*, 7578; b) A. Z. Nelson, R. E. Bras, J. Liu, R. H. Ewoldt, *J. Rheol.* **2018**, *62*, 357.
[8] a) V. Vogel, M. Sheetz, *Nat. Rev. Mol. Cell Biol.* **2006**, *7*, 265; b) J. Y. Lim, H. J. Donahue, *Tissue Eng.* **2007**, *13*, 1879; c) A. M. Pekkanen, R. J. Mondschein, C. B. Williams, T. E. Long, *Biomacromolecules* **2017**, *18*, 2669.
[9] A. Badea, J. M. McCracken, E. G. Tillmaand, M. E. Kandel, A. W. Oraham, M. B. Mevis, S. S. Rubakhin, G. Popescu, J. V. Sweedler, R. G. Nuzzo, *ACS Appl. Mater. Interfaces* **2017**, *9*, 30318.
[10] G. H. McKinley, T. Sridhar, *Annu. Rev. Fluid Mech.* **2002**, *34*, 375.
[11] A. L. Rutz, K. E. Hyland, A. E. Jakus, W. R. Burghardt, R. N. Shah, *Adv Mater* **2015**, *27*, 1607.
[12] M. N. Jones, *J. Colloid Interface Sci.* **1967**, *23*, 36.
[13] G. Laput, X. A. Chen, C. Harrison, *Proc. of the 28th Annual ACM Symp. on User Interface Software & Technology*, ACM, New York **2015**.
[14] H. Zhang, G. C. Hardy, Y. Z. Khimyak, M. J. Rosseinsky, A. I. Cooper, *Chem. Mater.* **2004**, *16*, 4245.
[15] C. J. Ferguson, R. J. Hughes, D. Nguyen, B. T. T. Pham, R. G. Gilbert, A. K. Serelis, C. H. Such, B. S. Hawkett, *Macromolecules* **2005**, *38*, 2191.
[16] Z. H. Zhou, J. Wang, X. Liu, H. S. O. Chan, *J. Mater. Chem.* **2001**, *11*, 1704.
[17] E. J. Park, J. K. Sim, M.-G. Jeong, H. O. Seo, Y. D. Kim, *RSC Adv.* **2013**, *3*, 12571.
[18] N. S. Tomer, F. Delor-Jestin, L. Frezet, J. Lacoste, *Open J. Org. Polym. Mater.* **2012**, *02*, 13.
[19] D. Xu, L. Sun, H. Li, L. Zhang, G. Guo, X. Zhao, L. Gui, *New J. Chem.* **2003**, *27*, 300.
[20] B. C. Smith, *Infrared Spectral Interpretation: A Systematic Approach*, CRC Press, Boca Raton, FL **1998**.
[21] L. Rösch, P. John, R. Reitmeier, *Silicon Compounds, Organic*, Ullmann's Encyclopedia of Industrial Chemistry, Wiley-VCH, Weinheim, Germany **2000**.
[22] Z. Wang, A. A. Volinsky, N. D. Gallant, *J. Appl. Polym. Sci.* **2014**, *131*, 41050.
[23] S. Kawaguchi, G. Imai, J. Suzuki, A. Miyahara, T. Kitano, K. Ito, *Polymer* **1997**, *38*, 2885.
[24] Q. D. Nguyen, D. V. Boger, *Annu. Rev. Fluid Mech.* **1992**, *24*, 47.
[25] C. W. Macosko, *Rheology Principles, Measurements, and Applications*, Wiley, New York **1994**.